REPORT DOCUMENTATION PAGE

Form Approved
OMB No. 0704-0188

1. AGENCY USE ONLY *(Leave blank)*	2. REPORT DATE	3. REPORT TYPE AND DATES COVERED
	August 1992	Technical Memorandum

4. TITLE AND SUBTITLE
Design and Experimental Validation of a Flutter Suppression Controller for the Active Flexible Wing

5. FUNDING NUMBERS
WU 505-64-20-01

6. AUTHOR(S)
Martin R. Waszak and S. Srinathkumar

7. PERFORMING ORGANIZATION NAME(S) AND ADDRESS(ES)
NASA Langley Research Center
Hampton, VA 23681-0001

8. PERFORMING ORGANIZATION REPORT NUMBER
L-16977

9. SPONSORING/MONITORING AGENCY NAME(S) AND ADDRESS(ES)
National Aeronautics and Space Administration
Washington, DC 20546-0001

10. SPONSORING/MONITORING AGENCY REPORT NUMBER
NASA TM-4381

11. SUPPLEMENTARY NOTES
Waszak: Langley Research Center, Hampton, VA; Srinathkumar: National Aeronautical Laboratory, Bangalore, India.

12a. DISTRIBUTION/AVAILABILITY STATEMENT
Unclassified–Unlimited

Subject Category 08

12b. DISTRIBUTION CODE

13. ABSTRACT *(Maximum 200 words)*
The synthesis and experimental validation of an active flutter suppression controller for the Active Flexible Wing wind-tunnel model is presented. The design is accomplished with traditional root locus and Nyquist methods using interactive computer graphics tools and extensive simulation-based analysis. The design approach uses a fundamental understanding of the flutter mechanism to formulate a simple controller structure to meet stringent design specifications. Experimentally, the flutter suppression controller succeeded in simultaneous suppression of two flutter modes, significantly increasing the flutter dynamic pressure despite modeling errors in predicted flutter dynamic pressure and flutter frequency. The flutter suppression controller was also successfully operated in combination with another controller to perform flutter suppression during rapid rolling maneuvers.

14. SUBJECT TERMS	15. NUMBER OF PAGES
Flutter suppression; Active control; Active flexible wing	17
	16. PRICE CODE A03

17. SECURITY CLASSIFICATION OF REPORT	18. SECURITY CLASSIFICATION OF THIS PAGE	19. SECURITY CLASSIFICATION OF ABSTRACT	20. LIMITATION OF ABSTRACT
Unclassified	Unclassified		

Abstract

The synthesis and experimental validation of an active flutter suppression controller for the Active Flexible Wing wind-tunnel model is presented. The design is accomplished with traditional root locus and Nyquist methods using interactive computer graphics tools and extensive simulation-based analysis. The design approach uses a fundamental understanding of the flutter mechanism to formulate a simple controller structure to meet stringent design specifications. Experimentally, the flutter suppression controller succeeded in simultaneous suppression of two flutter modes, significantly increasing the flutter dynamic pressure despite modeling errors in predicted flutter dynamic pressure and flutter frequency. The flutter suppression controller was also successfully operated in combination with another controller to perform flutter suppression during rapid rolling maneuvers.

Introduction

Modern aircraft designs emphasize the reduction of structural weight to maximize efficiency and agility. Reduced structural weight, however, results in reduced stiffness and increases the likelihood of structural dynamic instabilities (flutter). Active flutter suppression is an attractive solution to the problems associated with reduced weight. Developing methods to suppress flutter and reduce structural loads by utilizing active control systems was an objective of the Active Flexible Wing (AFW) program.

The AFW program was a joint venture between NASA Langley Research Center and Rockwell International, North American Aircraft. The program occurred in two phases. Only the second phase, which focused on active flutter suppression, will be addressed herein. Two wind-tunnel tests were conducted during the second phase. These tests were performed in the Transonic Dynamics Tunnel (TDT) at NASA Langley with a wind-tunnel model of the Active Flexible Wing (see fig. 1) that was built and supported by Rockwell. The goals of the AFW program were to develop and apply advanced control system design and analysis methodologies to flutter suppression and maneuver load control. The program objectives as they pertain to flutter suppression were to (1) develop mathematical aeroelastic models

L-89-12445

Figure 1. AFW wind-tunnel model mounted in TDT.

of the wind-tunnel model, (2) design and implement control systems to perform active flutter suppression and verify controller performance by means of wind-tunnel experiments, and (3) develop analysis tools to compare experimental and analytical controller performance (Noll et al. 1989).

This paper focuses on the design and wind-tunnel test of an active flutter suppression (AFS) system. The operation of the flutter suppression controller in steady flight and while performing rapid rolling maneuvers is specifically addressed. Developing such a system requires a mathematical model that accurately describes aeroelastic behavior, an understanding of the physical phenomena involved, and the ability to analyze the behavior of the system in the context of likely model errors. The role each of these aspects played in accomplishing the program objectives will be discussed herein with an emphasis on developing an understanding of key physical phenomena through a variety of analysis methods.

Characterization of AFW Wind-Tunnel Model in Flutter

Wind-Tunnel Model and Digital Controller

The AFW wind-tunnel model, depicted in figure 1, is an actively controlled, statically and aeroelastically scaled, full-span wind-tunnel model of an advanced tailless fighter aircraft. The fuselage is rigid, and the wings are flexible. The vehicle is supported by a sting with a ball bearing and brake mechanism that allows the vehicle to be fixed relative to the sting axis or free to roll about it (i.e., roll brake on and roll brake off, respectively). Four control surfaces, controlled by hydraulic actuators, are located on each wing semispan: leading edge outboard (LEO), leading edge inboard (LEI), trailing edge outboard (TEO), and trailing edge inboard (TEI). Only three of these surfaces (LEO, TEO, and TEI) were effective for flutter suppression. The vehicle is extensively instrumented with accelerometers, strain gauges, rotary variable differential transducers, and a rate gyro. Of particular interest for active flutter suppression are the four accelerometers on each wing semispan. Three of the accelerometers are located near the hinge line of the LEO, TEO, and TEI control surfaces near the surface midspan, and one is located near the wingtip at about midchord. A more detailed description of the wind-tunnel model is presented in Noll et al. (1989) and Miller (1988).

The active flutter suppression controller consists of a digital computer running at 200 samples per second and a variety of other electronic equipment that allows the digital computer to interface with the wind-tunnel model. In addition to computing the control system commands, the controller samples the analog vehicle responses, converts them to digital signals, and converts the digital control system outputs to analog control surface commands. The analog measurements are prefiltered by a first-order, 25-Hz antialiasing filter and can also be passed through notch filters (though this capability was not used in the control law described herein). A schematic diagram of the AFW wind-tunnel model and controller is depicted in figure 2. A detailed description of the digital controller is presented in Hoadley et al. (1991).

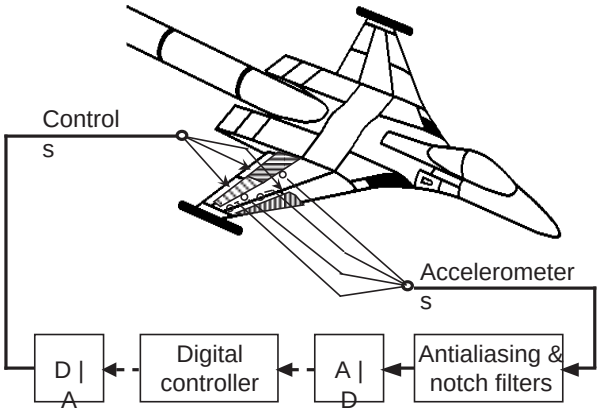

Figure 2. Schematic of AFW wind-tunnel model and AFS controller.

Mathematical Model

The mathematical model of the AFW wind-tunnel model used for control law synthesis and analysis consists of representations of the structural and aerodynamic characteristics, the control surface actuator dynamics, wind-tunnel turbulence, and the digital controller dynamics (including the processing required to transfer signals to and from the vehicle). A detailed description of the mathematical model can be found in Buttrill and Houck (1990).

The structural representation was developed by Rockwell and was provided to NASA Langley Research Center in a form that consisted of a lumped mass matrix and a structural influence coefficient matrix. The mass and stiffness information was used to compute a set of in vacuo vibration mode shapes, frequencies, and generalized masses for the 10 lowest frequency elastic modes for both symmetric motion and antisymmetric motion. The structural vibration modes were generated for both the roll brake on configuration and the roll brake off configuration. The model was then modified to match natural vibration

frequencies measured during ground vibration tests. Effective modal viscous damping of 1.5 percent was assumed, since structural damping was not addressed in the structural modeling process. The modal information was then used to compute linear unsteady aerodynamics.

The aerodynamic representations were generated with the Interaction of Structures, Aerodynamics, and Controls (ISAC) computer codes (Newsom et al. 1984 and Peele and Adams 1979). ISAC utilizes modal characteristics of the structure and a doublet lattice lifting surface method to compute unsteady aerodynamic force coefficients for a set of reduced frequencies for a given Mach number. The unsteady aerodynamic force coefficients at the various reduced frequencies were used to generate the rational function approximations that were then used to formulate mathematical models of the vehicle. The methods by which this was accomplished are documented in Noll et al. (1989) and Tiffany and Adams (1988).

The control surface actuator representations were generated with parameter estimation techniques to match frequency response data obtained by experiment. The experimental results indicate that the actuators could be accurately modeled over a wide frequency range, containing the predicted flutter frequency, by third-order transfer functions with no numerator dynamics. Each actuator has a unique transfer function such that corresponding left- and right-side control surfaces have different actuator models. This is the primary source of asymmetry in the mathematical model. However, individual control surface rate and deflection limits were also modeled.

Within the mathematical model, the digital controller was represented by a set of difference equations to characterize the dynamic compensation and by a set of differential equations to characterize the antialiasing filters. Representations of analog-to-digital and digital-to-analog converters and quantization effects were also part of the controller model.

The complete mathematical model of the AFW wind-tunnel model was obtained by combining the structural, aerodynamic, control surface actuator, and digital controller representations described above. The model was implemented with the Advanced Continuous Simulation Language (ACSL) computer program (Anon. 1987). The linear equations of motion for the structural dynamics, unsteady aerodynamics, and controller dynamics are included. In addition, nonlinearities associated with control surface deflection limits, actuator rate limits, and quantization effects were characterized. The effects of wind-tunnel turbulence were also incorporated into the simulation model by using an appropriately calibrated Dryden spectrum representation (Buttrill and Houck 1990).

Linear models, used extensively in the control system design and analysis process, were obtained by linearizing the ACSL model about equilibrium points at various conditions. Linear models were also obtained directly from ISAC. By generating linear models that addressed different boundary conditions (e.g., roll brake status), wind-tunnel operating conditions (e.g., dynamic pressure), modeling assumptions (e.g., number of modes, number of aerodynamic lags), etc., many issues regarding controller performance and robustness could readily be considered. This capability was extremely helpful in achieving the design goals.

Flutter Mechanism

The predicted symmetric dynamic characteristics of the AFW wind-tunnel model are summarized by the dynamic pressure root loci presented in figure 3. The root loci describe the variation in pole and zero locations with variations in dynamic pressure of the open-loop transfer function associated with symmetric tip accelerometer response due to symmetric TEO actuator command. The upper plot depicts the loci of all the symmetric structural modes contained in the model, while the lower plot depicts a close-up of the flutter region. These root loci are representative of all the control surface and accelerometer pairs when symmetric deformations are considered. The root loci are also representative of the flutter behavior for antisymmetric structural deformations with the roll brake on.

The root loci in figure 3 predicted that the AFW wind-tunnel model would exhibit classical wing bending/torsion flutter (Bisplinghoff and Ashley 1962). The flutter mode is characterized by coupling between the first wing bending mode and the first wing torsion mode. At low dynamic pressures these two modes are distinct with characteristic bending and torsion mode shapes. As the dynamic pressure increases, these two modes become coupled so that the bending and torsion modal frequencies tend to coalesce to a common frequency and take on mode shapes that exhibit characteristics of both wing bending and wing torsion. Eventually, one mode becomes unstable and manifests itself as a divergent oscillation displaying both bending and torsion motions.

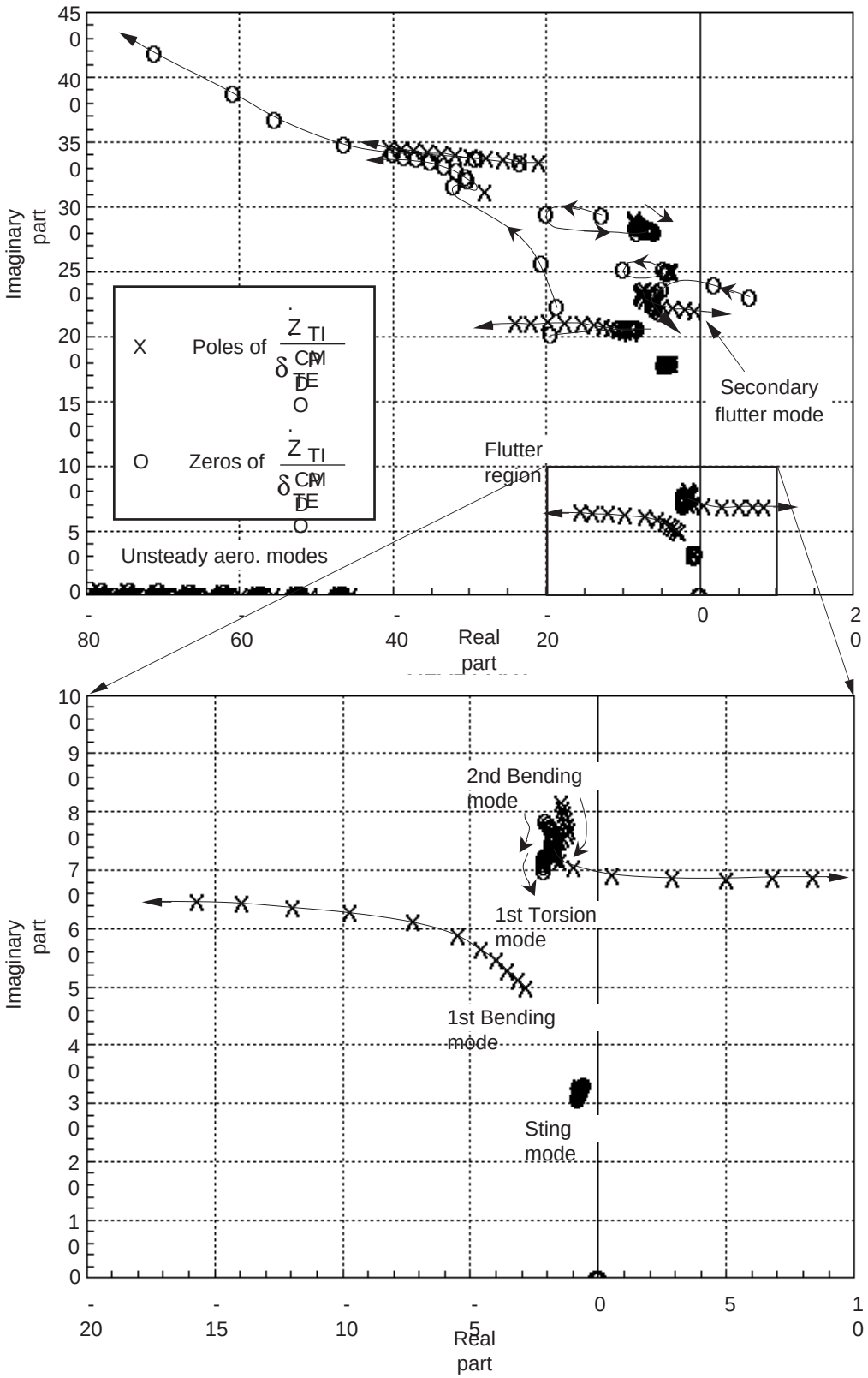

Figure 3. Symmetric dynamic pressure root loci; open loop. Dynamic pressure range: 100–350 psf, 25 psf intervals; $\ddot{Z}_{\mathrm{TIP}}$ is the tip accelerometer response and $\delta_{\mathrm{TEO}}^{\mathrm{CMD}}$ is the commanded trailing-edge outboard control surface deflection.

With the roll brake on, the AFW wind-tunnel model exhibits two distinct flutter modes (symmetric and antisymmetric) within the operating range of the Transonic Dynamics Tunnel (TDT) in which the AFW wind-tunnel model was tested. The mathematical model predicted that the flutter modes would have similar flutter frequencies (symmetric—11.2 Hz; antisymmetric—10.9 Hz) and similar flutter dynamic pressures (symmetric—248 psf; antisymmetric—233 psf). The flutter dynamic pressures and flutter frequencies of the wind-tunnel model differ somewhat from these predictions, as will be seen. There is a secondary symmetric flutter mode that is predicted to occur at a frequency of approximately 35 Hz. This was cause for some concern but, since the maximum attainable dynamic pressure of the wind tunnel was approximately 300 psf, no attempt was made to stabilize or otherwise affect the secondary symmetric flutter mode.

When the model is free to roll, only symmetric flutter is predicted to occur within the operating range of the TDT. Consequently, only a symmetric mode controller is used when the model is free to roll. In addition, the predicted symmetric flutter behavior is the same regardless of whether the roll brake is on or off and so the same controller can potentially be used in both cases.

Control System Design

Design Objectives and Specifications

The basic objective of the flutter suppression controller was to maintain stability over the widest possible dynamic pressure range. Maintaining stability implies that flutter will be suppressed at dynamic pressures above that of open-loop flutter and that the controller will not destabilize the model at dynamic pressures below that of open-loop flutter. Limitations on the operating conditions for the TDT significantly restricted the verifiable increase in flutter dynamic pressure afforded by active flutter suppression. The difference between the predicted flutter dynamic pressure of the AFW wind-tunnel model and the maximum dynamic pressure attainable with the TDT (approximately 300 psf at a Mach number of about 0.5) translates into a maximum verifiable increase in predicted flutter dynamic pressure of approximately 29 percent. The design objective was, therefore, to increase the flutter dynamic pressure by more than 30 percent. In addition, the flutter suppression system was required to perform in the presence of wind-tunnel turbulence and subject to uncertainty in the design model.

An additional objective was to perform rapid rolling maneuvers while simultaneously performing flutter suppression. This required the concurrent operation of both an AFS controller and a rolling maneuver controller. The specific objective was to suppress flutter while performing a rolling maneuver satisfying scaled military specifications for time to roll 90° (i.e., perform a 90° roll, starting from rest, in less than 0.4 sec).

Design specifications were developed to reflect required levels of robustness. Gain and phase margins of ± 4 dB and $\pm 30°$, respectively (or their multivariable equivalents), were required over the entire operating range to account for modeling errors and uncertainties. However, gain and phase margins may not effectively characterize system robustness for some forms of modeling error and uncertainty (Maciejowski 1989). As a result, sensitivity analyses were required to assure that likely modeling errors and uncertainty effects could be accommodated by the AFS controller.

Additional design specifications were established to address the limited rate capability of the control surface actuators. The peak (aerodynamically) unloaded rate limit for the actuators was conservatively chosen to be approximately 150 deg/sec. To reduce the probability of rate limiting, the rms commanded actuator rate was required to be less than one third the maximum achievable rate, about 50 deg/sec in this case. If the commanded control surface deflection occurs predominantly at the flutter frequency, then the corresponding maximum allowable rms commanded control surface deflection is approximately 0.7°.

The controller was also limited by the requirement to operate at a sampling rate of 200 Hz. As a result, the controller had to be simple enough that all required computations could be completed in 0.005 sec. This was particularly crucial when simultaneously performing flutter suppression and roll control, since the same control computer had to perform both functions.

Design Philosophy and Approach

The basic design philosophy for the AFS system was to devise the simplest controller structure that met all the design goals. A low-complexity controller allows the designer to retain the ability to readily identify the relationships between the open-loop system dynamics and the effects of feedback. It also increases the likelihood of meeting computational requirements.

Developing a simple control structure required a fundamental understanding of the flutter mechanism.

This involved identifying the key features of the transition to flutter (as depicted in fig. 3) and the basic influence of feedback. Once this understanding was developed, the design approach was to systematically choose the appropriate inputs and outputs, and add dynamic feedback compensation to meet the desired objectives.

Implementation Issues

A key step in the control design process was to identify aspects of the open-loop dynamics that were of value in performing active flutter suppression. For instance, only the control surfaces that were most effective in controlling the flutter modes were considered. Similarly, only those sensors most able to sense the flutter motion were considered. This significantly simplified the controller synthesis by eliminating those controls and measurements that had little potential for helping to meet the objectives.

The predicted control surface characteristics are such that the trailing edge inboard and outboard surfaces are much more effective in controlling flutter than the leading edge surface. The TEO surface was predicted to be most effective at controlling the first wing bending mode, while the TEI surface was predicted to be most effective at controlling the first wing torsion mode. In addition, the LEO surface actuator has hinge moment limitations due to destabilizing aerodynamic loading that limit the usefulness of that surface. Therefore, only the two pairs of trailing edge surfaces were considered.

The accelerometer characteristics are such that, while each accelerometer is fairly responsive to the flutter modes, only the tip accelerometer demonstrates desirable high-frequency roll-off. The other accelerometers are considerably more sensitive to high-frequency modes and would require additional filtering to generate the required high-frequency roll-off. The phase lags and the added complexity associated with this additional filtering were deemed undesirable. As a result, the tip accelerometer ($\ddot{Z}_{\mathrm{TIP}}$) was the only sensor used in the design.

Finally, an approach was required to simultaneously stabilize the two distinct flutter modes. Since both symmetric and antisymmetric flutter were predicted to occur at similar frequencies and dynamic pressures when the roll brake was on, coupling effects had to be assessed. The primary source of coupling was slight asymmetry in the control surface actuators, though deflection and rate limits were also included in the mathematical model. The lack of strong coupling in the mathematical model allowed the two flutter modes to be treated independently; that is, separate control laws for each flutter mode were designed.

Addressing these implementation issues prior to control law synthesis allowed the general controller structure, with eight possible inputs and six possible outputs controlling both flutter modes, to be simplified to a controller structure with two decoupled control laws, each suppressing a single flutter mode, using one input and two outputs. Also, the similarity of the two flutter modes was exploited by using the same controller structure to suppress both symmetric and antisymmetric flutter. The significant reduction in complexity resulting from this process was a key factor in the success of the AFS controller.

Controller Synthesis

The controller synthesis process is similar to that used by Schmidt and Chen (1986). The basic tools used in the AFS process were root locus and Nyquist plots. The application of interactive computer graphics was instrumental in addressing a variety of complex issues influencing controller performance. In addition, analyses of the AFW/AFS system were performed with both the simulation model and linear models to address performance and robustness issues. The simulation model was used whenever nonlinearities were suspected to have a potential impact.

Inspection of the dynamic pressure root loci for the tip acceleration due to TEO surface deflection (fig. 3) reveals that the flutter mechanism depends primarily on two structural modes. These modes, their associated zeros, and the two zeros at the origin associated with the use of acceleration feedback are all that is required to effectively characterize the flutter mechanism. Two additional modes in the same frequency range (sting mode and second bending mode) play a secondary role. The large frequency separation between the flutter region and the other vehicle dynamics allows the higher order dynamics to be neglected during the design process. However, the impact of the dynamics outside the flutter region on system performance must be determined once the preliminary control system design is complete. If the performance is significantly degraded, the design may need to be modified.

The first step in the synthesis procedure was to assess the impact of using proportional feedback (without additional compensation) to stabilize the flutter modes. This was accomplished by considering a single flutter mode (e.g., symmetric motion, roll brake on) using a single input/output pair (namely, wingtip accelerometer and TEO control surface). The objective was not necessarily to use proportional feedback

exclusively, but to develop insight into the control mechanism and assess the problems that would likely occur in attempting to employ a simple solution.

The pole-zero constellation depicted in figure 4 represents the key features of the flutter mechanism described above. Two gain root loci can result during attempts to stabilize this system with proportional feedback once flutter has occurred. One locus is stabilizing and the other is nonstabilizing. Which of the two loci occurs depends on the relative position of the poles and zeros of the subject transfer function. The controller must produce a stabilizing locus for all the pole and zero positions associated with variations in dynamic pressure (both below and above flutter), and for perturbations in their locations due to modeling errors.

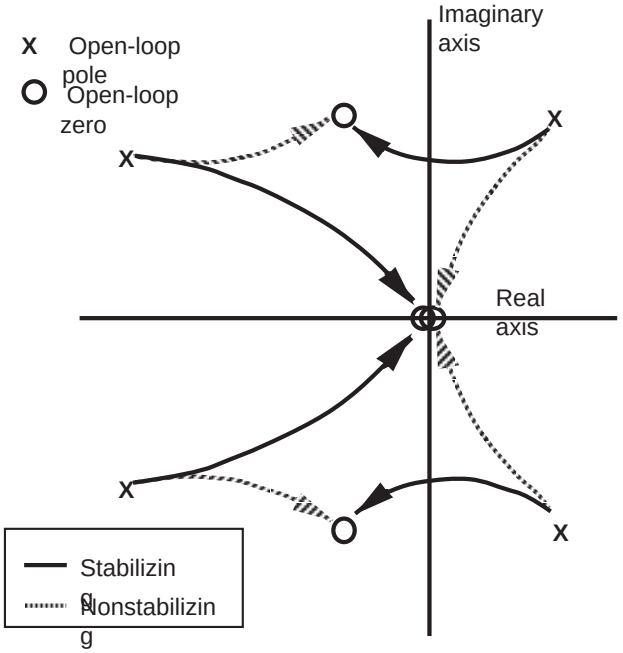

Figure 4. Possible gain root loci for flutter mechanism.

The positions of the lightly damped complex conjugate zeros shown in figure 4 are critical in determining whether the root locus that occurs is stabilizing or nonstabilizing. These "critical" zeros are also responsible for the relatively large gain required to stabilize the system by using proportional feedback. The large gain required for stabilization is undesirable mainly because of its effect on higher frequency dynamics. While the flutter mode can be stabilized, the large gain can easily cause higher frequency poles to become unstable. Dynamic compensation is therefore required to assure that the stabilizing root locus is achieved (subject to plant variations and modeling errors) and that the feedback gain can be small enough to assure that high-frequency poles remain stable.

Root locus concepts were used to develop a third-order filter structure that accomplishes the above objectives. The filter is characterized by a pair of complex conjugate poles near the "critical" zeros, an associated pair of highly damped complex conjugate zeros, and a first-order washout filter. The filter transfer function structure is

$$\frac{u(s)}{y(s)} = K\frac{s}{s+p}\frac{(s+a+jb)(s+a-jb)}{(s+c+jd)(s+c-jd)} \qquad (1)$$

where $u(s)$ is the output and $y(s)$ is the input to the filter.

The washout filter pole was chosen to assure that undesired low-frequency disturbances and measurement biases were sufficiently attenuated. The complex conjugate poles were placed in locations near, but clearly to the left of, the "critical" zeros. This assures that the resulting pole/zero interaction causes the desired stabilizing root locus path to be achieved, even when subjected to moderate plant variations and modeling errors. The complex conjugate zeros were placed well into the left half plane at a damped natural frequency slightly above that of the complex conjugate poles. The specific location of the zeros resulted from attempting to simultaneously maximize the gain and phase margins of the system.

The filter structure described above provides a simple control law that allows the flutter mode to be stabilized. However, there are several conflicting design objectives (e.g., increasing flutter dynamic pressure, robustness to dynamic pressure variations, robustness to modeling errors, and control surface actuator limits) that must be met for the controller to be successful. These objectives were met by modifying the pole and zero placements and the filter gain and by combining the effects of the TEO and TEI control surfaces. It was in this phase of the design that interactive computer graphics were used extensively. The pole and zero placements were chosen by a combination of root locus and Nyquist analyses. The gain values were chosen primarily by Nyquist analysis and simulation to equalize the positive and negative gain margins over a wide range of dynamic pressures. Recall that the symmetric flutter behavior is independent of whether or not the roll brake is engaged. Therefore, the same filter was used to suppress symmetric flutter regardless of whether or not the model was free to roll. It was also found that, for the symmetric controller, the TEI surface had little impact on the controller performance. As a result, only the TEO surface was used for symmetric flutter.

The final set of AFS controller parameters that were used in the flutter suppression controller are

$$\left.\begin{aligned} K &= 0.4871 \text{ deg/g} \\ p = 5, a &= 40, b = 75, c = 7, d = 70 \end{aligned}\right\} \quad (2)$$

A frequency response plot of this filter is shown in figure 5. Note that the control law resembles an inverted notch filter, since it amplifies signals over a narrow frequency range. This characteristic allows the unstable plant pole to be stabilized with a gain sufficiently small that higher order plant dynamics are not significantly affected. Note also that there is no roll-off in the filter. This characteristic is acceptable because the desired roll-off is provided by the first order, 25-Hz antialiasing filter and by the high-frequency attenuation associated with the tip accelerometer response.

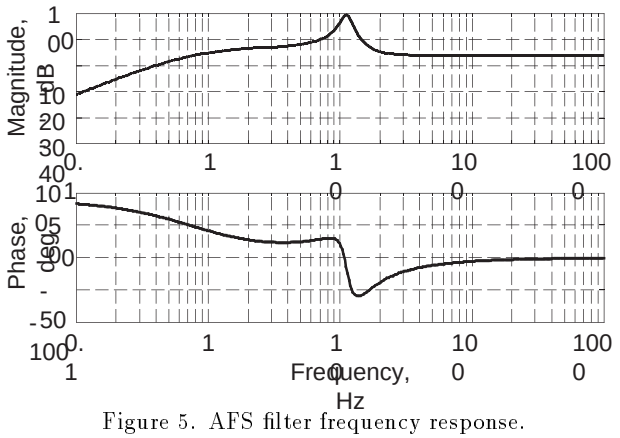

Figure 5. AFS filter frequency response.

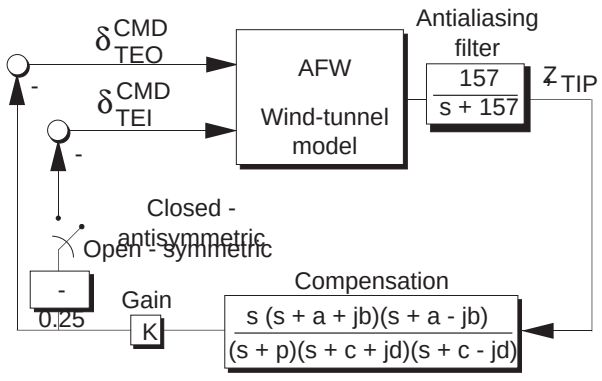

Figure 6. AFS controller block diagram.

The same filter parameters (eqs. (2)) were used to suppress the antisymmetric flutter mode when the roll brake was on. This was possible because of the similarity of the flutter mechanisms of the two flutter modes. It was found, however, that the TEO and TEI surfaces were both effective in controlling the antisymmetric flutter mode. As a result, both trailing-edge control surfaces were used. The controller was no more complicated, however, because the two surfaces were driven by the same controller command with a gain ratio of -0.25. This ratio was determined by parametric simulation studies and resulted in improved stability margins compared with those obtained by using the TEO surface exclusively. A block diagram representation of the AFS controller implementation is presented in figure 6.

Integration With Rolling Maneuver Controllers

The AFS controller was designed independently from the rolling maneuver controller. However, issues associated with simultaneously performing flutter suppression and rapid rolling maneuvers were considered in the AFS design. The bandwidth required to perform rolling maneuvers was of sufficiently low frequency that the commands of the roll controllers could be treated as disturbances to the AFS controller. (The controllers used to perform rapid rolling maneuvers had bandwidth requirements below 1 Hz, while the predicted flutter dynamics were at frequencies above 10 Hz.) The washout filter, included in the AFS controller structure to attenuate biases and low-frequency disturbances, provided the required attenuation.

A major concern was the potential for the two controllers to compete for control power. When a control surface reaches its deflection or rate limit, the closed-loop transfer function for the rate-limited surface effectively becomes instantaneously open loop. If this situation occurs above the open-loop flutter boundary for sufficiently long periods of time, flutter may occur. However, if control is only lost or degraded momentarily, stability can be maintained.

Deflection limits were placed on the roll controller commands so that there would be sufficient control deflection capability for the AFS controller to perform its flight critical function. Rate limits could not be imposed in a similar manner, however, because of controller software and hardware constraints. As a result, the potential for rate limiting had to be addressed in the analysis of the AFS controller. Results from this analysis are presented in the next section. Fortunately, no severe problems emerged and the design did not require modification to allow rapid rolling maneuvers to be performed beyond the flutter boundary.

Closed-Loop Analysis

The predicted effect of applying the AFS controller to the AFW is summarized in the closed-loop

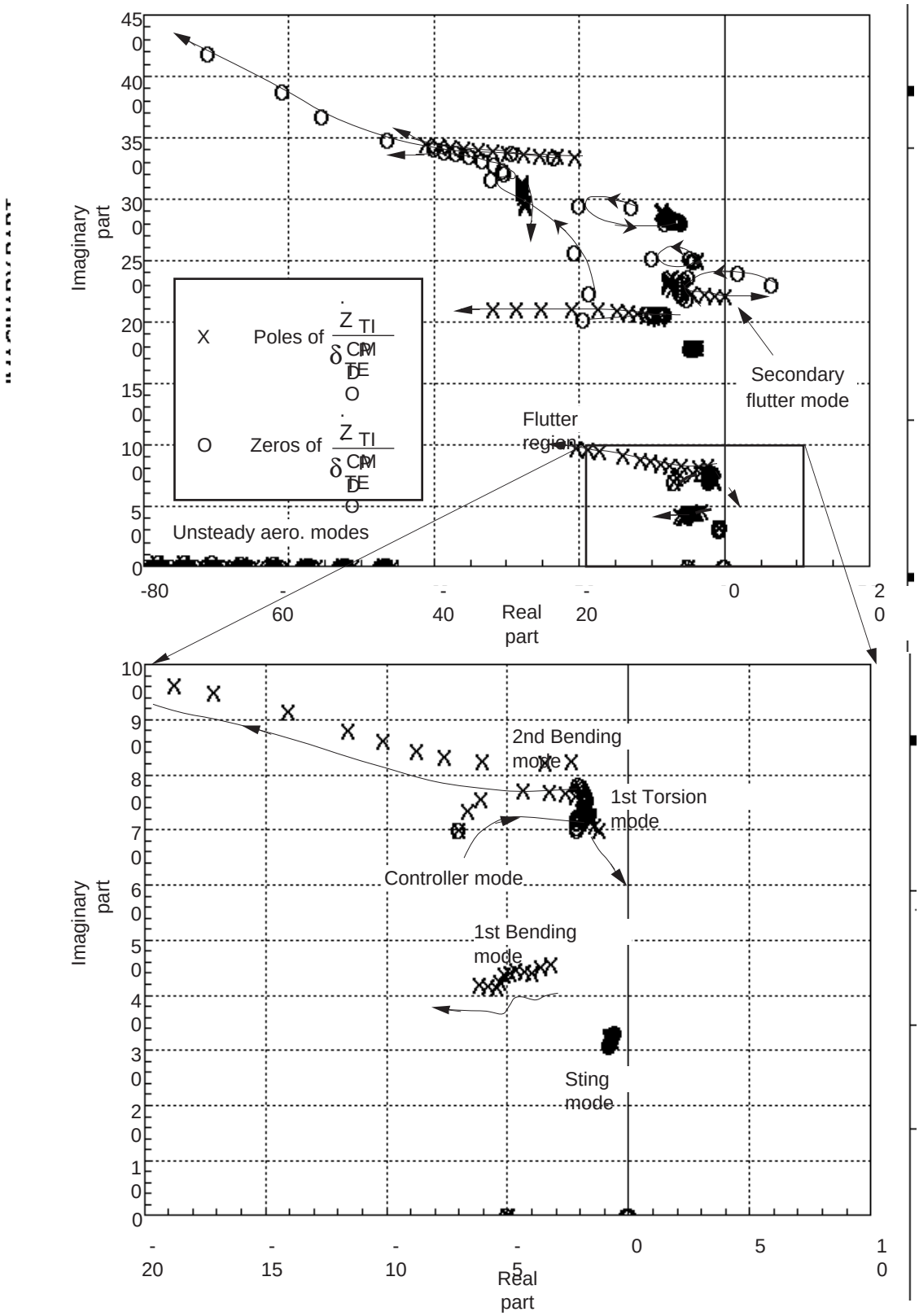

Figure 7. Symmetric dynamic pressure root loci; closed loop. Dynamic pressure range: 100–350 psf, 25 psf intervals.

dynamic pressure root loci presented in figure 7. The AFS control law stabilizes the system over the desired range of dynamic pressures. The closed-loop system becomes unstable at a dynamic pressure between 325 and 350 psf. Recall that the control law was designed to suppress the primary flutter mode without affecting the higher frequency dynamics. A comparison of the open-loop and closed-loop dynamic pressure root loci reveals that this objective was met. The difference between the open-loop and closed-loop root loci is primarily restricted to the flutter region. Differences at higher frequencies are limited to minor perturbations. One notable difference between the open-loop and closed-loop root loci at high frequencies is the dynamic pressure at which a pole associated with the secondary symmetric flutter mode (at a frequency of about 35 Hz) moves into the right half plane. In the open-loop case, the secondary flutter mode becomes unstable at a dynamic pressure of slightly over 350 psf, while in the closed-loop case this occurs at a dynamic pressure between 325 and 350 psf. This was cause for some concern but, since the maximum attainable dynamic pressure of the wind tunnel was approximately 300 psf, no attempt was made to stabilize or otherwise affect the secondary symmetric flutter mode.

Once the basic AFS control system design was established, various analyses were performed to assess the ability of the controller to meet the design objectives.

Stability Margins and Control Activity

Figure 8 summarizes the results of the stability margin analyses. The symmetric and antisymmetric controllers both satisfy the ±4 dB gain margin and ±30° phase margin specifications over a range of dynamic pressures from 100 to 325 psf. At dynamic pressures above 325 psf the gain margins drop below the specified ±4 dB, but the required phase margins are still achieved.

Control surface activity, especially deflection rate, due to wind-tunnel turbulence was a major concern in the design process, since the actuator limitations place significant restrictions on attainable performance. Figure 9 summarizes the analytically predicted control surface activity for a range of dynamic pressures with the model free to roll (roll brake off). These predicted values were obtained with a batch simulation of the nonlinear mathematical model with the antisymmetric control law disengaged. The required control surface activity is below the maximum allowable (0.7°, 50 deg/sec) over the dynamic pressure range from 100 to 300 psf. The control surface rate required for roll brake off at a dynamic pressure of 315 psf, however, is slightly above the maximum. The control activity with the roll brake on is similar.

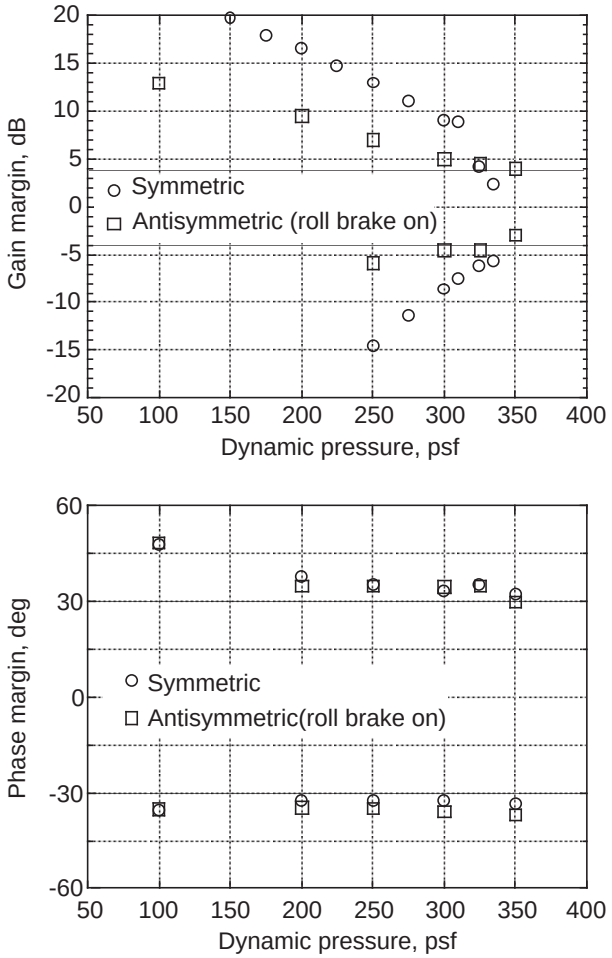

Figure 8. Predicted stability margins.

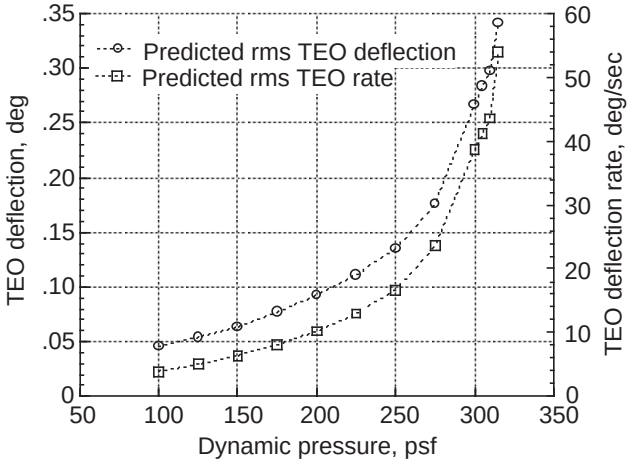

Figure 9. Predicted rms control surface activity (roll brake off).

Table I. Sensitivity to Aeroelastic Frequency and Control Effectiveness—Symmetric Mode

[Dynamic pressure = 300 psf]

ΔGain = −4 dB

ω_b	ω_τ −10%	ω_τ Nominal	ω_τ +10%
−10%	*S	S	S
Nominal	S	S	S
+10%	U	U	S

ΔGain = 0 dB

ω_b	ω_τ −10%	ω_τ Nominal	ω_τ +10%
−10%	S	S	S
Nominal	S	S	S
+10%	U	S	S

ΔGain = +4 dB

ω_b	ω_τ −10%	ω_τ Nominal	ω_τ +10%
−10%	S	S	S
Nominal	S	S	S
+10%	U	S	S

*Representative of experimentally observed parameter errors.
ω_b = Bending mode frequency
ω_τ = Torsion mode frequency
S = Stable
U = Unstable

Sensitivity and Robustness to Modeling Errors

In addition to the basic stability margin and control activity analysis, sensitivity analyses were performed to address the impact of specific forms of modeling error. The first sensitivity analysis addressed the effects of simultaneous variations in the aeroelastic frequencies of the two structural modes that lead to flutter and variations in control effectiveness approximated by perturbations in the controller gain. The results of this analysis for the symmetric mode are presented in table I.

The analysis involved using the simulation model to evaluate the stability of the closed-loop system at a dynamic pressure of 300 psf subject to simultaneous ±10-percent variations in the frequencies of the two key aeroelastic modes. This was accomplished by separating the aerodynamic stiffness terms from the in vacuo vibration frequencies and modifying only the aerodynamic stiffness. The control gain was varied by ±4 dB to represent variations in control effectiveness. This analysis suggests that the symmetric controller is somewhat sensitive to a simultaneous increase in the bending mode frequency and decrease in the torsion mode frequency. The instability associated with the lower left-hand matrix elements in table I denotes this sensitivity.

A sensitivity analysis was also performed to determine the effect of variations in structural damping. The AFS controller was implemented with a version of the AFW simulation model in which the structural damping was reduced to zero. At a dynamic pressure of 300 psf and with all other model parameters nominal, the reduction in structural damping had no noticeable effect. Therefore, moderate variations in structural damping were predicted to have no significant impact on controller performance.

Another analysis was performed to address the performance of the AFS controller during rolling maneuvers. The main concerns were the likelihood and impact of rate limiting. When the model is free to roll, the antisymmetric AFS control channel is open. Consequently, the AFS controller generates only symmetric commands, whereas the rolling controller generates purely antisymmetric commands to produce the rolling maneuvers. The mathematical model assumes no coupling between the symmetric and antisymmetric dynamics except through asymmetric actuator effects and saturation of individual actuators.

The approach to assess possible interactions was to consider the impact of a worst-case scenario. The AFS system uses the TEO surface as its primary control. The deflection limits imposed on the rolling maneuver controller commands are ±10°. In addition, the typical rolling maneuver involves initiating a roll, sustaining it for a short period, and then stopping in less than 1.0 sec from the time of initiation. Based on these factors, a worst-case roll command (from the perspective of the AFS) was chosen to be a 10° doublet to the TEO surface with a period of about 1.0 sec.

The simulation of the AFW wind-tunnel model was driven by the roll doublet and wind-tunnel turbulence while the AFS controller was operating at a dynamic pressure of 300 psf. Some rate limiting did

occur, but only on one side of the AFW wind-tunnel model at a time and only for very short periods on the order of 0.05 sec. When the roll command required maximum control surface rate (to initiate or stop the roll), one TEO surface moved up and the other moved down (antisymmetrically) at the rate limit. The symmetric flutter suppression controller simultaneously commanded control deflections that caused both TEO control surfaces (left and right) to move in the same direction (symmetrically). As a result, the side that was commanded by both controllers to move in the same direction experienced rate limiting. The other surface, however, could still operate below the rate limit. The implication is that the flutter suppression controller never becomes completely ineffective due to rate limiting. It does, however, momentarily lose some effectiveness since it is, in effect, only operating on one side of the vehicle at a time. The AFS controller had no difficulty maintaining system stability subject to these simulated conditions. This indicates that the available gain margins are sufficient to sustain stability subject to the worst-case effect of rolling maneuvers.

The sensitivity analysis results presented above indicate that the AFW controller met all the design goals and specifications. The analysis results also provided a considerable amount of insight into the likely behavior of the system at nonideal operating conditions. Both the analysis results and the acquired insight provided the designers with information that was useful during the wind-tunnel test to troubleshoot problems and evaluate the implications of experimental results.

Wind-Tunnel Tests

Two wind-tunnel tests were performed with the AFS controller. The first test (fall 1989) was aimed at performing plant estimation, flutter clearance tests, and validating the performance of active flutter suppression controllers and roll maneuver controllers individually. The second test (winter 1991) was aimed at more extensive flutter suppression and roll maneuver control tests, and validating the combination of flutter suppression and rolling maneuver control. The following discussion summarizes the test results in terms of the accuracy of the mathematical model and the performance of the AFS system operating alone and in combination with the rolling maneuver controller.

Accuracy of the Mathematical Model

Plant identification was performed during both wind-tunnel tests. Figure 10 presents two representative transfer function plots for the wingtip accelerometer response due to symmetric TEO commanded control surface deflection. The first plot corresponds to a dynamic pressure of 175 psf, which is well below the flutter dynamic pressure. The second plot corresponds to a dynamic pressure of 275 psf, which is well above the flutter dynamic pressure. The corresponding responses for the mathematical model are shown for comparison. In both cases there is general agreement; however, there are also notable differences between the experimental data and the analytical results. One of the most significant differences is the shift in the frequencies of the key aeroelastic modes. The frequencies of the two modes that characterize the flutter behavior (first bending and first torsion) occur at roughly 1.5 Hz below the predicted values over a range of dynamic pressures from 175 to 275 psf. As a result, symmetric flutter occurs at approximately 9.6 Hz rather than 11.2 Hz as predicted. Similar discrepancies occurred for the antisymmetric mode.

Another difference between the analytical and experimental frequency responses is the peak magnitude. The differences in the vicinity of the flutter frequency range from 2 to 5 dB for dynamic pressures from 175 to 275 psf. As a result, the predicted control effectiveness was somewhat greater than was measured. This effect was even more pronounced for the antisymmetric frequency responses.

Differences between the mathematical model and the experimental results also occurred at the dynamic pressure associated with the onset of flutter. Analysis of the mathematical model predicted that symmetric and antisymmetric flutter would occur at dynamic pressures of approximately 248 and 233 psf, respectively. The actual symmetric and antisymmetric flutter dynamic pressures are 235 and 219 psf, respectively.

The differences between the mathematical model and the actual vehicle were a cause for concern. Fortunately, the AFS controller was robust to errors in both control effectiveness and flutter frequency, particularly in the observed combinations as shown in the results from the sensitivity analysis in table I. The shaded region corresponds to simultaneous reduction in control effectiveness and reduction in bending and torsion mode aeroelastic frequencies.

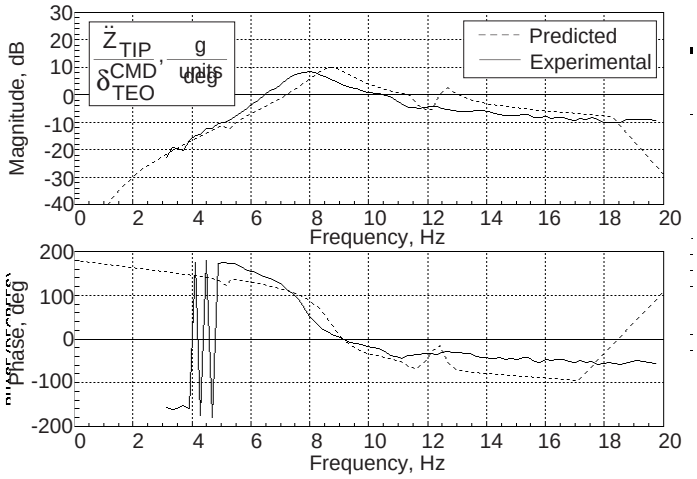

(a) Symmetric mode; Dynamic pressure = 175 psf.

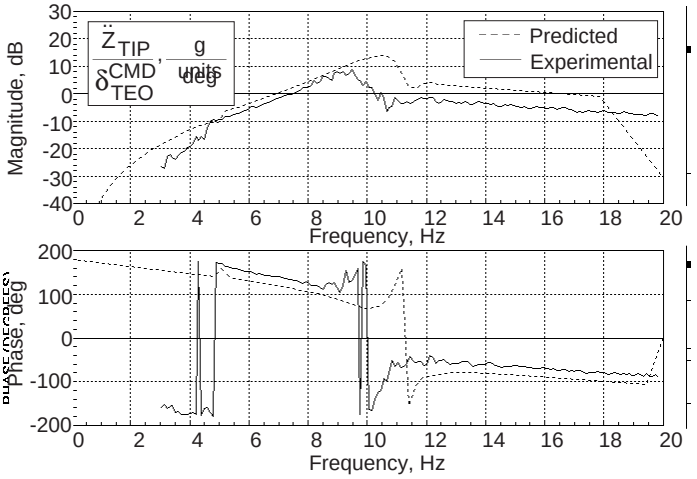

(b) Symmetric mode, Dynamic pressure = 275 psi.

Figure 10. Frequency response comparison: predicted and experimental.

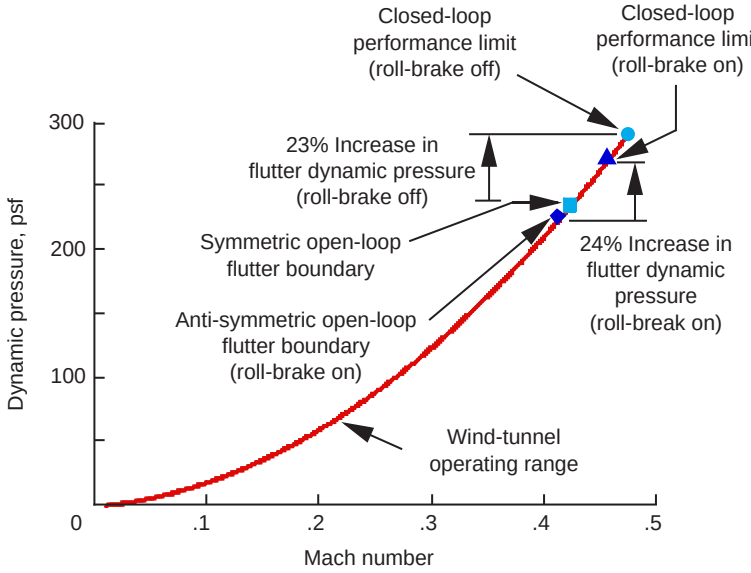

Figure 11. Flutter suppression test results.

Flutter Suppression Performance

Figure 11 summarizes the performance of the AFS controller in suppressing the single symmetric flutter mode when the vehicle was free to roll and in simultaneously suppressing two flutter modes (symmetric and antisymmetric) when the vehicle was fixed in roll. The flutter dynamic pressure was increased by over 24 percent when the roll brake was on and by over 23 percent when the roll brake was off.

With the roll brake on, oscillatory structural deflections caused loads that were in excess of preset safety limits. These loads occurred at a dynamic pressure of 272 psf, at which point testing was curtailed. The experimental data suggest that the controller stability limit had not been reached, in that the controller was providing sufficient damping to maintain stability. The oscillations, though sustained enough to exceed the safety limits, were stable.

With the roll brake off, the maximum dynamic pressure of the wind tunnel (290 psf) was reached, and so further increases in dynamic pressure were impossible. However, the system was performing as predicted. Extrapolation of the experimental data indicated that the dynamic pressure could have been increased to approximately 330 psf before instability would occur. It should be noted, however, that safety limits would likely have been exceeded before the stability limit could be attained, as was the case when the roll brake was on.

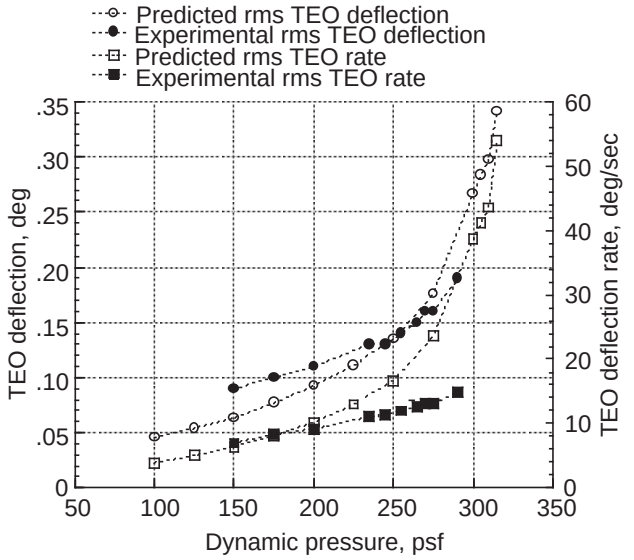

Figure 12. Rms control surface activity: predicted and experimental (roll brake off).

The control activity that was required to achieve the demonstrated levels of flutter suppression was less than half the design requirement. Figure 12 presents the actual and predicted rms control activity for the free-to-roll case (symmetric control law only). The peak rms control rate was less than 20 deg/sec, which is considerably less than predicted. This is an indication that the turbulence model used in the control synthesis was somewhat conservative. It is possible that higher gains might have been used. However, the gain values were chosen more on obtaining uniform stability margins than on limiting control activity. Higher gains would also likely lead to smaller stability margins, which would be undesirable.

Another measure of performance of the AFS controller is the level of stability indicated by the Nyquist plots depicted in figure 13. Nyquist plots for the AFW/AFS system at three dynamic pressures are presented: 175 psf, which is well below open-loop flutter; 225 psf, which is very close to open-loop flutter; and 275 psf, which is well beyond open-loop flutter. These plots show that the controller succeeds in meeting the stability margin requirements and exhibits good robustness properties over a wide range of dynamic pressures. The results show that the stability margins of the AFS controller were acceptable for dynamic pressures below 275 psf. The gain margins are well in excess of the ± 4 dB required. The positive phase margins exceed the requirement and the predicted values, but the negative phase margins are slightly smaller in magnitude than $-30°$. A comparison of the experimental and predicted results shows similar margins despite the modeling errors, an indication of the robustness of the controller.

Flutter Suppression With Roll Maneuvering

The AFS controller was combined with a rolling maneuver controller (Moore et al. 1990) to demonstrate the ability to perform flutter suppression while performing rapid rolling maneuvers. The test involved performing rapid rolling maneuvers over a range of dynamic pressures both below and above flutter. At a dynamic pressure of 260 psf (25 psf beyond flutter), the rolling controller was able to achieve acceptable rapid rolling maneuvers. The flutter suppression controller had no difficulty maintaining stability, and the control activity and vehicle responses suggest no significant differences between the AFS performance in either steady or maneuvering flight.

Concluding Remarks

The success of the Active Flexible Wing (AFW) program demonstrates the feasibility of using active control systems to suppress violent flutter both in steady flight and while performing aggressive rolling

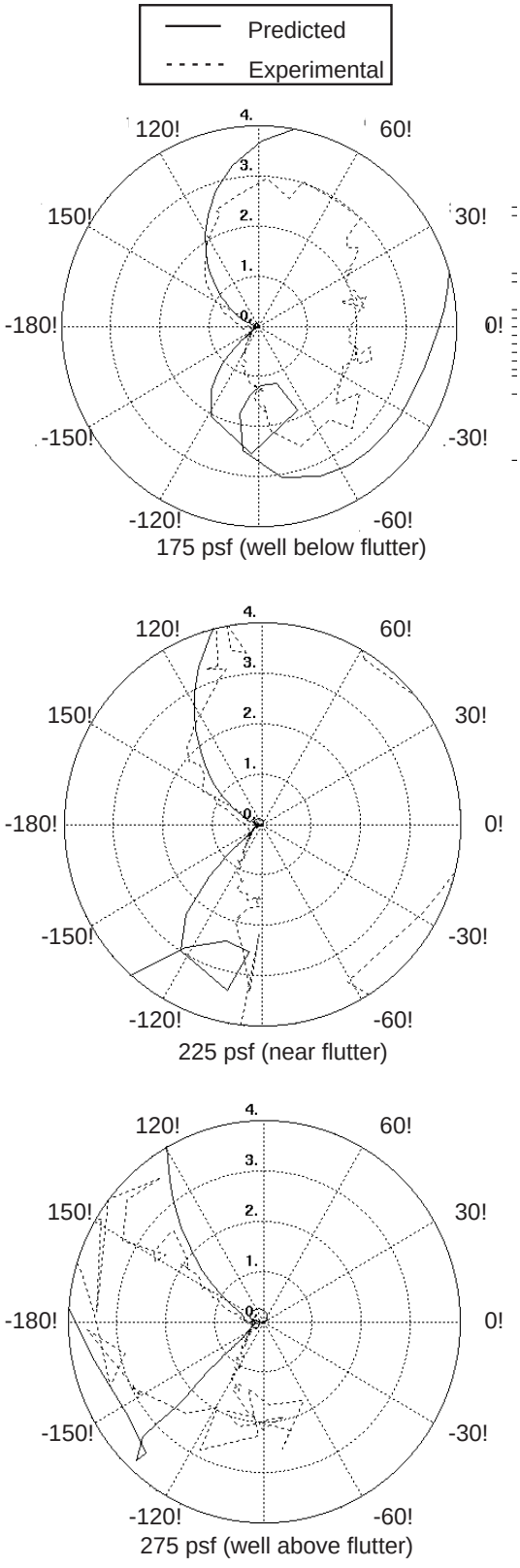

Figure 13. Nyquist plots for AFW/AFS system: symmetric mode.

maneuvers representative of high-performance military aircraft. These accomplishments were achieved despite significant errors in predicted control effectiveness, flutter frequency, and flutter dynamic pressure in the mathematical model, which nevertheless accurately characterized the flutter mechanism. The design approach exploited a fundamental understanding of the flutter mechanism and used a simple structure with inherent robustness properties and resulted in a controller that was relatively insensitive to the key modeling errors. This study, therefore, emphasized the importance of considering robustness to modeling errors in the control system design process and of developing models that accurately characterize the physical phenomena.

Unfortunately, the wind-tunnel model will not be available for future wind-tunnel tests. However, the AFW program results provide an excellent basis for investigating aeroelastic phenomena and for the development and validation of aeroservoelastic systems. The mathematical models, the extensive body of measured data including transfer functions and flutter characteristics, and the experience gained by those involved in the study, make the AFW an excellent candidate for future work.

NASA Langley Research Center
Hampton, VA 23681-0001
July 17, 1992

References

Anon. *Advanced Continuous Simulation Languages (ACSL)—Reference Manual.* Mitchell and Gauthier Assoc., c.1987.

Bisplinghoff, Raymond L.; and Ashley, Holt: *Principles of Aeroelasticity.* Dover Publ., Inc., c.1962.

Buttrill, Carey S.; and Houck, Jacob A.: *Hot-Bench Simulation of the Active Flexible Wing Wind-Tunnel Model.* NASA TM-102758, 1990.

Hoadley, Sherwood T.; Buttrill, Carey S.; McGraw, Sandra M.; and Houck, Jacob A.: Development, Simulation Validation, and Wind-Tunnel Testing of a Digital Controller System for Flutter Suppression. *4th NASA Workshop on Computational Control of Flexible Aerospace Systems,* Lawrence W. Taylor, Jr., compiler, NASA CP-10065, Part 2, 1991, pp. 583–613.

Maciejowski, Jan Marian: *Multivariable Feedback Design.* Addison-Wesley, c.1989.

Miller, Gerald D.: *Active Flexible Wing (AFW) Technology.* AFWAL-TR-87-3096, U.S. Air Force, Feb. 1988.

Moore, D. B.; Miller, G. D.; and Klepl, M. J.: Roll Plus Maneuver Load Alleviation Control System Designs for the Active Flexible Wing Wind Tunnel Model. *4th NASA Workshop on Computational Control of Flexible*

Aerospace Systems, Lawrence W. Taylor, Jr., compiler, NASA CP-10065, Part 2, 1991, pp. 561–582.

Newsom, J. R.; Adams, W. M., Jr.; Mukhopadhyay, V.; Tiffany, S. H.; and Abel, I.: Active Controls: A Look at Analytical Methods and Associated Tools. *ICAS Proceedings 1984—14th Congress of the International Council of the Aeronautical Sciences,* B. Laschka and R. Staufenbiel, eds., International Council of the Aeronautical Sciences, 1984, pp. 230–242.

Noll, Thomas E.; Perry, Boyd, III; Tiffany, Sherwood H.; Cole, Stanley R.; Buttrill, Carey S.; Adams, William M., Jr.; Houck, Jacob A.; Srinathkumar, S.; Mukhopadhyay, Vivek; Pototzky, Anthony S.; Heeg, Jennifer; McGraw, Sandra M.; Miller, Gerald; Ryan, Rosemary; Brosnan, Michael; Haverty, James; and Klepl, Martin: *Aeroservoelastic Wind-Tunnel Investigations Using the Active Flexible Wing Model—Status and Recent Accomplishments.* NASA TM-101570, 1989.

Peele, Ellwood L.; and Adams, William M., Jr.: *A Digital Program for Calculating the Interaction Between Flexible Structures, Unsteady Aerodynamics and Active Controls.* NASA TM-80040, 1979.

Schmidt, D. K.; and Chen, T. K: Frequency Domain Synthesis of a Robust Flutter Suppression Control Law. *J. Guid., Control, and Dyn.,* vol. 9, no. 3, May–June 1986, pp. 346–351.

Tiffany, Sherwood H.; and Adams, William M., Jr.: *Nonlinear Programming Extensions to Rational Function Approximation Methods for Unsteady Aerodynamic Forces.* NASA TP-2776, 1988.

Table I. Sensitivity to Aeroelastic Frequency and Control Effectiveness—Symmetric Mode

[Dynamic pressure = 300 psf]

ΔGain = -4 dB

	ω_τ		
ω_b	-10%	Nominal	$+10\%$
-10%	*S	S	S
Nominal	S	S	S
$+10\%$	U	U	S

ΔGain = 0 dB

	ω_τ		
ω_b	-10%	Nominal	$+10\%$
-10%	S	S	S
Nominal	S	S	S
$+10\%$	U	S	S

ΔGain = $+4$ dB

	ω_τ		
ω_b	-10%	Nominal	$+10\%$
-10%	S	S	S
Nominal	S	S	S
$+10\%$	U	S	S

*Representative of experimentally observed parameter errors.

ω_b = Bending mode frequency

ω_τ = Torsion mode frequency

S = Stable

U = Unstable